Journal Name

ARTICLE

Dramatic impact of the TiO_2 polymorph on the electrical properties of 'stoichiometric' $Na_{0.5}Bi_{0.5}TiO_3$ ceramics prepared by solid-state reaction

Received 00th January 20xx,
Accepted 00th January 20xx

DOI: 10.1039/x0xx00000x

www.rsc.org/

Fan Yang[a,#,*], Yidong Hu[b,#], Qiaodan Hu[b,*], Sebastian Steiner[c], Till Frömling[c,*], Linhao Li[d], Patrick Wu[d], Emilio Pradal-Velázquez[d] and Derek C Sinclair[d,*]

Bulk conductivity (σ_b) values of nominally stoichiometric $Na_{0.5}Bi_{0.5}TiO_3$ (NBT) prepared by solid-state reaction collated from literature show random variation between 10^{-6} -10^{-3} S cm^{-1} (at 600 °C). This makes it challenging to obtain reliable and reproducible performances of NBT-based devices, especially as the underlying reason(s) for this variance are not fully understood. Here we report the dramatic impact of the TiO_2 reagent, in particular, the polymorphic form of TiO_2 on the electrical conductivity and conduction mechanism of NBT. Based on our solid-state processing route, NBT ceramics prepared by rutile TiO_2 are ionically conductive, and those prepared by anatase TiO_2 are insulating. The dramatic difference in electrical properties of NBT prepared using rutile and anatase TiO_2 is related to the NBT formation process: the intermediate phase $Bi_{12}TiO_{20}$ is more stable during formation of NBT in the case of anatase TiO_2, which reduces the volatility of Bi_2O_3 during solid-state reaction. These results give plausible explanations for the large variation of σ_b reported in the literature and highlight the importance of selecting an appropriate TiO_2 reagent when targeting controllable σ_b in NBT-based ceramics. For ion-conducting applications (such as in intermediate-temperature solid oxide fuel cells, IT-SOFCs), rutile TiO_2 should be used, and for dielectric applications (such as in multilayer ceramic capacitors, MLCC) anatase TiO_2 should be used.

Introduction

Sodium bismuth titanate ($Na_{0.5}Bi_{0.5}TiO_3$, NBT) has been long considered as a promising lead-free piezoelectric/ferroelectric material to replace lead zirconate titanate (PZT) [1,2], and therefore has potential applications in sensors, actuators, and multi-layer ceramic capacitors[3]. It is also a recently discovered oxide-ion conductor, which shows great potential as an electrolyte material for intermediate-temperature solid oxide fuel cells (IT-SOFCs)[4,5]. Different applications require totally different electrical properties of NBT. For example, for dielectric/ferroelectric applications, a low bulk electrical conductivity (σ_b) is essential to reduce the leakage current and dielectric loss. In contrast, for IT-SOFCs applications, a high σ_b is required to reduce the ohmic polarization. However, σ_b of NBT is highly sensitive to small compositional variations such that very low levels of Na or Bi non-stoichiometry can lead to significant changes in σ_b[4, 5]. σ_b of NBT, in particular, the nominally stoichiometric NBT ($NB_{0.50}T$) reported by different research groups can vary several orders of magnitude, i.e., σ_b <10^{-6} S cm^{-1} (600 °C) by Khatua *et al.*[6] and σ_b ~ 10^{-3} S cm^{-1} (600 °C) by Li *et al.*[4]. A summary of values for NBT collated from the literature[4-13] is plotted in Fig.1, where significant scattering of σ_b can be observed. This variance of σ_b makes it challenging to obtain reliable and reproducible performances of NBT-based devices.

Previous studies[4, 5] have revealed the significant change in σ_b induced by low levels of Na or Bi non-stoichiometry (<1 at.%) as being related to a switch between electronic and oxide-ion conduction. Similar behavior can be observed using varying concentrations of acceptor dopants[9, 14]. The presence of a small number of oxygen vacancies can change the predominant intrinsic electronic conduction behavior of NBT based on a d^0 insulator to predominant oxide-ion conduction due to the high mobility of oxygen ions in the NBT lattice[15]. Dense NBT ceramics are usually prepared by the conventional solid-state reaction method using Na_2CO_3, Bi_2O_3, and TiO_2 as reagents. Although different researchers may employ a different procedure, a general route for solid-state reaction synthesis involves pre-drying, weighing, milling, calcination, cold pressing, and sintering. Many steps in this process can cause low-level compositional variations and thus influence the oxygen vacancy level and therefore alter the σ_b of NBT. Over several years, we have conducted careful investigations to probe the relationships between the solid-state processing procedure and the electrical behaviour of NBT and have established a "standard" route to minimize the impact from sample preparation to obtain controllable σ_b. Under our "standard" route, σ_b and the conduction mechanism can be flexibly tuned by varying the A-site Na/Bi ratio of the starting composition. When Na/Bi ≥ 1, i.e., Na-excess or Bi-deficient, NBT exhibits high σ_b

[a.] Institute of Fuel Cells, School of Mechanical Engineering, Shanghai Jiao Tong University, 200240, Shanghai, China. Email: fanyang_0123@sjtu.edu.cn;
[b.] School of Materials Science and Engineering, Shanghai Jiao Tong University, 200240, Shanghai, China. Email: qdhu@sjtu.edu.cn;
[c.] Department of Materials and Earth Science, Technical University of Darmstadt, FB Nichtmetallisch-Anorganische Werkstoffe, Alarich-Weiss-Straße 2, D-64287 Darmstadt, Germany. Email: froemling@ceramics.tu-darmstadt.de;
[d.] Department of Materials Science and Engineering, University of Sheffield, S1 3JD, UK. Email: d.c.sinclair@sheffield.ac.uk
[#] These authors contribute equally.

with an oxide-ion transport number, t_{ion} close to unity at ≥ 600 °C. When Na/Bi <1, i.e., Na-deficient or Bi-excess, NBT shows very low σ_b with t_{ion} close to zero at ≥ 600 °C. A detailed discussion on the defect chemistry mechanisms induced by A-site Na or Bi non-stoichiometry and how they affect the electrical properties of NBT can be found in Ref. 16.

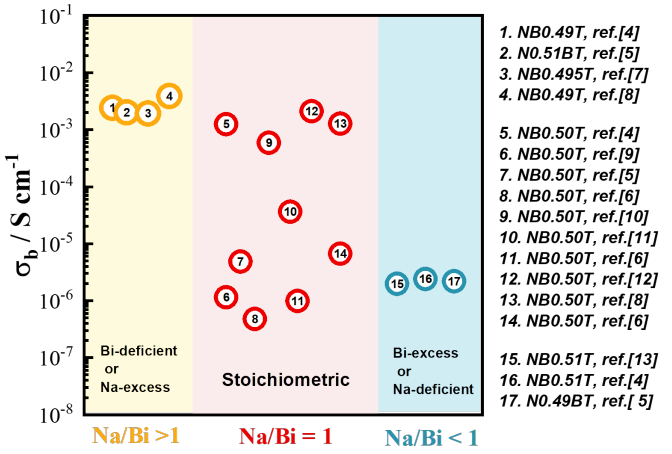

Fig.1 Summary of σ_b for NBT ceramics based on various Na/Bi ratios. Data are collated from the literature.

It should be noted that the above-mentioned empirical relationship between σ_b and Na/Bi ratio is established based on using the same Na_2CO_3 (99.5%), Bi_2O_3 (99.9%), and TiO_2 (99.9%, rutile) reagents. The high sensitivity of σ_b to compositional variations highlights the possibility that reagents with different purity grades, types of impurity, or those from different suppliers (or different batches from the same supplier), may also have a significant impact on σ_b of NBT. Such concerns are not unfounded as low levels of impurities have been proven to have dramatic effects on the electrical properties of many perovskite-type materials such as $BaTiO_3$[17] and $LaFeO_3$[18]. Furthermore, the common polymorphic phase of the TiO_2 reagent, i.e., rutile or anatase, may also have an impact on σ_b of NBT. This has been overlooked previously because the anatase to rutile phase transition of undoped TiO_2 usually occurs between 600-700 °C[19]. In our "standard" solid-state processing procedure, TiO_2 powder is subjected to pre-treatment overnight drying at 900 °C prior to weighing and batching. It is considered to have fully transformed to the rutile form after pre-drying; however, the TiO_2 polymorphic phase transition temperature can vary over a wide temperature range ~ 400-1200 °C depending on variables such as impurities, dopants, particle morphology, and synthesis method[20]. It is possible that anatase TiO_2 can be retained after pre-drying at 900 °C. Recently, Goutham *et al.*[21] reported the significantly dissimilar microstructural and dielectric/ferroelectric properties of NBT synthesized with anatase and rutile TiO_2 via a hydrothermal technique. Whether and how different phases of TiO_2 impact the electrical conductivity of NBT prepared by solid-state reaction has yet to be explored.

Here we investigate the effect of raw starting materials on the electrical properties of NBT ceramics prepared by solid-state reaction. Raw reagents from different suppliers with reasonable grade purity (> 99.5%) were selected to prepare nominally stoichiometric $NB_{0.50}T$ ceramics by our "standard" route. We show the polymorphic form of the TiO_2 source has a dramatic impact on the electrical properties of $NB_{0.50}T$. The possible reasons for the significantly different electrical conductivity behaviour of $NB_{0.50}T$ prepared by anatase and rutile TiO_2 are investigated and discussed. This work provides a plausible explanation for the large variance within the literature regarding the reported electrical properties of NBT-based materials prepared by the solid-state reaction method. This suggests that anatase should be used as the pre-dried TiO_2 reagent to prepare NBT ceramics via solid-state synthesis for piezo/ferroelectric applications, and rutile TiO_2 to prepare NBT for ion-conducting applications, i.e., as electrolyte material for IT-SOFCs.

Experimental

Raw materials

Nominally stoichiometric NBT ($NB_{0.50}T$) ceramics were prepared by the conventional solid-state reaction method using Na_2CO_3, Bi_2O_3, and TiO_2 as starting materials. Raw materials with reasonable purity levels from various suppliers were used to evaluate the impact of different reagents. Detailed information on the raw reagents used is listed in Table 1.

The "standard" solid-state reaction route

All NBT ceramics were prepared by the same solid-state reaction route. Prior to weighing, the raw powders were dried overnight at 300 °C for Na_2CO_3 and Bi_2O_3 and 900 °C for TiO_2. Appropriate amounts of each reagent were weighed according to the chemical formula $Na_{0.5}Bi_{0.5}TiO_3$ and ball-milled in isopropanol using yttria-stabilized zirconia grinding media for 6 hours. The mixture was dried overnight in an 85 °C oven, sieved, and then calcined at 800 °C for 2 h. The resultant powder was subjected to a second round of ball milling (4 h), drying, sieving, and calcination (800 °C for 2 h) and subsequently to a final, third round of ball milling (6 h) and sieving. The products were compacted into pellets either by uni-axial cold pressing followed by isostatic pressing at 200 MPa, or by uni-axial pressing with a 5 wt.% water solution of polyvinyl alcohol (PVA) as a binder. Pellets were embedded in sacrificial powder of the same composition and sintered at 1150 °C for 2 h. The heating and cooling rates for calcination and sintering were 5 °C min^{-1}. Those with PVA binder were slowly heated to 550 °C with a heating rate of 2 °C min^{-1} and held for 2 h to decompose the binder before sintering. The use of a binder has little influence on the electrical conductivity and conduction mechanism of NBT, as shown by Fig.S1. After sintering, pellets were removed from the sacrificial powder and ground using SiC sandpaper to obtain flat surfaces.

Characterisations

Phase purity of NBT was examined by X-ray diffraction on the pellet surface using a Bruker D2 phaser. Ceramic microstructures were observed by scanning electron microscopy (SEM, JEOL JSM-6010LA, JEOL Ltd., Tokyo, Japan or Pheom XL, Netherlands) on thermally etched surfaces. Raman spectroscopy was performed using a Confocal Microprobe Raman system (Renishaw inVia Qontor, UK). Particle size distribution was analysed using a Mastersizer (S3500, Microtrac, USA). Atomic fractions of Na, Bi, and Ti in NBT ceramics were measured by Inductively Couple Plasma- Atomic Emission Spectroscopy (ICP-AES, Thermo Scientific™ iCAP7600, UK).

Electrical properties were measured by impedance spectroscopy using an Agilent E4980A impedance analyser (Agilent Technologies Inc., Palo-Alto, CA; frequency range 1 MHz to 20 Hz; 100 mV applied) or a Solartron 1260 system (Solartron Analytical, UK; frequency range 1 MHz to 0.01 Hz; 100 mV applied) using Au paste (fired at 850 °C for 2 h) or Pt paste (fired at 900 °C for 2 h) as electrodes. All impedance data were corrected for high frequency inductance associated with the leads and the measurement jig by performing a short circuit measurement. The corrected data were then normalised by a geometric factor (thickness/surface area) based on sample dimensions. Equivalent circuit fitting was performed using ZView software (Scribner Associates, Inc, Southern Pines, NC). Dielectric properties were measured using an LCR meter (Agilent E4980 Precision LCR Meter, Agilent Technologies) with an applied ac voltage of 100 mV. Data points were collected every 60 s from room temperature (RT) to 800 °C using a non-inductively wound tube furnace at a ramp rate of 1 °C min^{-1}.

Formation process of NBT

To study the formation of NBT during solid-state reaction, pre-dried Na_2CO_3, Bi_2O_3, and TiO_2 were weighed in the appropriate amounts and ball milled for 6 h. After drying, the mixed powders were heat treated between 400 – 800 °C (at 50 °C increments) for 2 h at each temperature. After cooling to room temperature, the resultant powder was subjected to laboratory XRD (D8 ADVANCE Da Vinci, Germany), synchrotron XRD (BL14B1 beam line station of Shanghai Synchrotron Radiation Facility, SSRF), and Raman spectroscopy (Renishaw inVia Qontor, UK) measurements to identify the reaction products. For the Synchrotron XRD experiments, a quartz capillary tube filled with calcined powder was fixed on a sample holder and aligned parallel to the X-ray beam. During measurements, an X-ray beam of 18 keV was applied to the sample with an exposure time of 20 s.

No.	Na_2CO_3	Bi_2O_3	TiO_2
1	99.5%, Fisher Chemical, UK	99.9%, Acros Organics, USA	99.9%, Sigma Aldrich, UK
2	99.5%, Alfa Aesar, Germany	99.975%, Alfa Aesar, Germany	99.6%, Alfa Aesar, Germany
3	99.8%, Aladdin, China	99.9%, Aladdin, China	99.9%, Alfa Aesar, China
4			99.99%, Aladdin, China

Results

To identify the possible impact from different reagents, a designed experiment was conducted to prepare 5 $NB_{0.50}T$ ceramics using a combination of Na_2CO_3, Bi_2O_3, and TiO_2 reagents from the first two rows of Table 1. These ceramics are denoted as NBT_111, NBT_112, NBT_211, NBT_121, and NBT_222, where 1 and 2 represent the row number. For example, NBT_111 represents the ceramic prepared by Na_2CO_3, Bi_2O_3, and TiO_2 from the first row, and NBT_121 by Na_2CO_3 from the first row, Bi_2O_3 from the second row, and TiO_2 from the first row, etc. By comparing the electrical conductivity of NBT_111 and NBT_112, the effect of TiO_2 can be evaluated. Similarly, effects of Na_2CO_3 and Bi_2O_3 can be analyzed by comparing σ_b of NBT_111 and NBT_211, and that of NBT_111 and NBT_121, respectively. After that, two more NBT ceramics were prepared using Na_2CO_3, Bi_2O_3, and TiO_2 reagents from the third and the fourth row of Table 1, denoted as NBT_333 and NBT_334. All NBT ceramics were dense (> 95%) and phase pure by laboratory XRD (Fig.S2).

The electrical properties of $NB_{0.50}T$ ceramics prepared using different combinations of Na_2CO_3, Bi_2O_3, and TiO_2 reagents from Table 1 are shown in Fig.2. The Z^* plots at 600 °C (Fig.2a) of these ceramics show two types of impedance responses. NBT_222, NBT_112, and NBT_334 show a single arc in Z* plots with an associated resistivity of > 10^5 Ω cm. The associated capacitance of the single arc is ~ 10^{-10} F cm^{-1}, corresponding to a relative permittivity (ε_r) of ~1000, which agrees well with the value for paraelectric NBT materials at this temperature[22]. Therefore, the single arc in the Z^* plots for NBT_222, NBT_112 and NBT_334 represent the bulk response. NBT_111, NBT_211, NBT_121, and NBT_333 show significantly smaller associated resistivity as indicated by the dashed rectangle in Fig.2a. An expanded view of the Z^* plots for these three ceramics show three arcs, Fig.2b. From high to low frequency and based on the magnitude of associated capacitances, these correspond to responses associated with bulk, grain boundary, and electrode effects, respectively. This is consistent with previous reports on the impedance response of ionically conductive NBT[4, 23, 24].

Bulk resistance (R_b) of these ceramics was obtained by equivalent circuit fitting of the impedance spectra using one *R-CPE* element for NBT_222, NBT_112, and NBT_334 (inset figure in Fig.2a), and three series-connected *R-CPE* elements for NBT_111, NBT_121, NBT_211, and NBT_333 (inset figure in Fig.2b). R_b was subsequently converted to σ_b (= $1/R_b$), and presented in Arrhenius plots (Fig.2c). NBT_222, NBT_112, and NBT_334, σ_b – $1000/T$ show a linear relationship with E_a ~ 1.7 eV, which is ~ half of the optical bandgap of NBT [25], suggesting predominant intrinsic electronic conduction behaviour. The σ_b – $1000/T$ relationships for NBT_111, NBT_121, NBT_211 and NBT_333, show a change in E_a from ~ 0.85 eV below 300 °C to ~ 0.40 eV above 300 °C. A change of E_a at ~ 300 °C is a characteristic of ionically conductive NBT.

The two distinct types of electrical behaviour associated with these NBT ceramics can also be demonstrated by the dielectric loss-temperature profiles (tan δ – T, 1 MHz). As shown in Fig.2d, NBT_222, NBT_112, and NBT_334 exhibit low tan δ over a wide temperature range (< 0.05 between 300 and 650 °C). On the contrary, tan δ for NBT_111, NBT_121, NBT_211, and NBT_333 shows a rapid increase in the intermediate temperature range (i.e., 300-400°C) and exceeds 0.2 at ~ 400 °C. The above results suggest, although prepared under an identical solid-state processing route, $NB_{0.50}T$ can still present significantly different σ_b and conduction mechanisms.

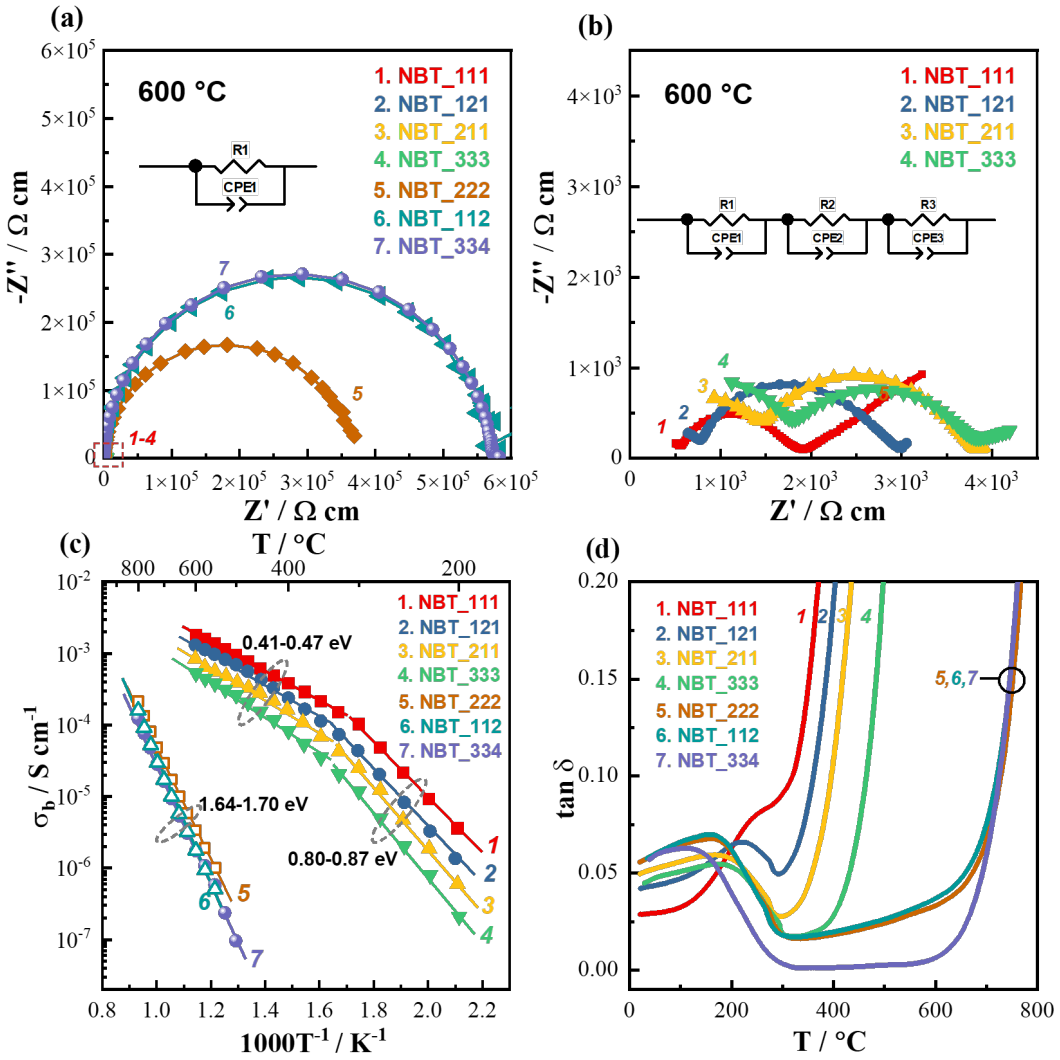

Fig.2 Electrical properties of $NB_{0.50}T$ ceramics prepared using different combinations of Na_2CO_3, Bi_2O_3, and TiO_2 reagents. (a) Z^* plots and the equivalent circuit for the fitting of impedance data for NBT_222, NBT_112, and NBT_334; (b) an expanded view of the dashed rectangular region in (a) showing Z^* plots for NBT_111, NBT_121, NBT_211, and NBT_333. The inset figure is the equivalent circuit used for fitting the data; (c) Arrhenius plots of σ_b. The numbers in eV are the activation energies (E_b) for σ_b; (d) tan δ – T plots at 1 MHz.

For a clearer illustration of the impact from different reagents, σ_b, E_a and the conduction mechanisms of these NBT ceramics are summarized in Table 2. The different Na_2CO_3 and Bi_2O_3 reagents produce only small variations in σ_b and E_a without changing the conduction mechanism. In contrast, using different TiO_2 reagents can induce a change in the conduction mechanism between predominantly oxide-ion and electronic conduction, and thus lead to 3 orders of magnitude variation in σ_b.

Table 2 Effect of reagents on the electrical properties of $NB_{0.50}T$ ceramics.

Effect	Sample	σ_b (600 °C) / S cm^{-1}	E_a / eV	Conduction mechanism
Na_2CO_3	NBT_111	0.0018	0.41 (> 300 °C) 0.80 (< 300°C)	Oxide-ion conduction
	NBT_211	8.34×10^{-4}	0.44 (> 300 °C) 0.85 (< 300°C)	Oxide-ion conduction
Bi_2O_3	NBT_111	0.0018	0.41 (> 300 °C) 0.80 (< 300°C)	Oxide-ion conduction
	NBT_121	0.0013	0.44 (> 300 °C) 0.82 (< 300°C)	Oxide-ion conduction
TiO_2	NBT_111	0.0018	0.41 (> 300 °C) 0.80 (< 300°C)	Oxide-ion conduction
	NBT_112	1.76×10^{-6}	1.75 (> 550 °C)	Electronic conduction
	NBT_333	5.25×10^{-4}	0.47 (> 300 °C) 0.87 (< 300°C)	Oxide-ion conduction
	NBT_334	1.75×10^{-6}	1.68 (> 550 °C)	Electronic conduction

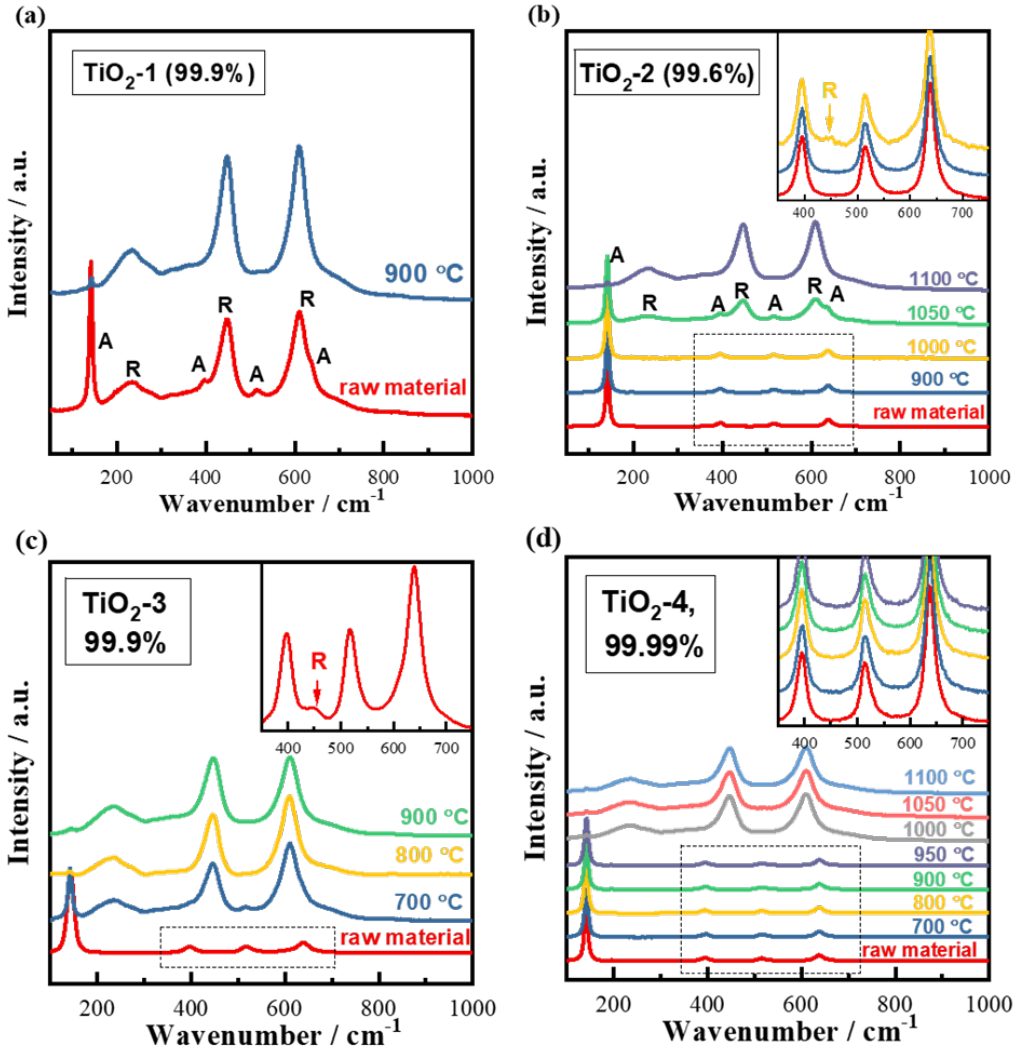

Fig.3 Raman spectra of the TiO_2 reagents before and after pre-drying at different temperatures. (a) TiO_2-1 (99.9%, Sigma Aldrich, UK); (b) TiO_2-2 (99.6%, Alfa Aesar, Germany); (c)TiO_2-3 (99.9%, Alfa Aesar, China) and (d) TiO_2-4 (99.99%, Aladdin, China). The inset figures in (b)-(d) are expanded views of the dashed rectangular regions. A and R denote anatase and rutile, respectively.

In our solid-state processing route, raw TiO_2 reagents are subjected to pre-drying at 900 °C for 8 h prior to weighing. For our NBT preparation, the starting phase is therefore rutile for TiO_2-1 and TiO_2-3 and anatase for TiO_2-2 and TiO_4-4. The significantly different electrical properties of $NB_{0.50}T$ ceramics prepared from different TiO_2 reagents may originate from 1) different purity levels of the TiO_2 and/or 2) different phases (rutile versus anatase). To identify the critical factors that influence the electrical conduction behaviour, σ_b and E_a of NBT prepared by different TiO_2 reagents (after pre-drying at 900 °C) are plotted as a function of purity of the TiO_2 reagents, Fig.4. NBT ceramics prepared using anatase TiO_2, with low purity (99.6%) and high purity (99.99%), show low σ_b (~10^{-6} S cm^{-1} at 600 °C) and high E_a (>1.6 eV); in contrast, those prepared using rutile TiO_2 with medium purity (99.9%) have high σ_b (~10^{-3} S cm^{-1} at 600 °C) and low E_a (~ 0.40 eV at > 300 °C and ~ 0.85 eV at < 300 °C). Compared to grade purity, the polymorphic form of TiO_2 has a determinant effect on the electrical conductivity and conduction mechanism of $NB_{0.50}T$ ceramics.

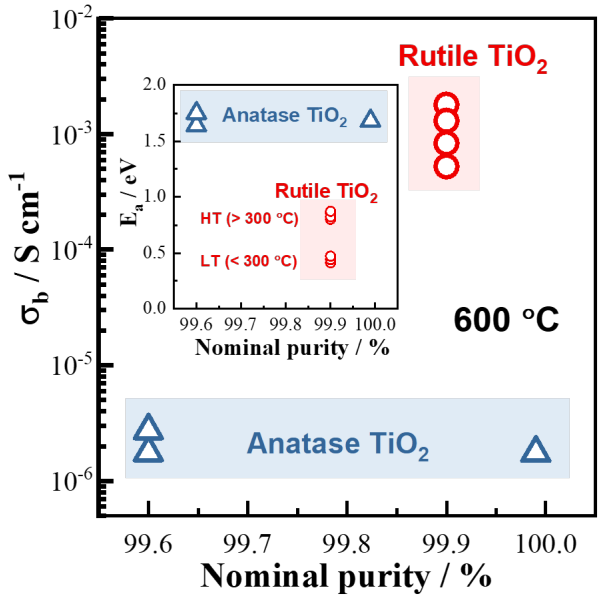

Fig.4 Variation of σ_b (at 600 °C) as a function of TiO_2 reagent purity. The inset figure is a plot of E_a versus TiO_2 reagent purity.

Discussion

The major discovery of this work is that the polymorphism of TiO_2 plays a critical role in the electrical conductivity and conduction mechanism of nominally stoichiometric NBT ($NB_{0.50}T$) ceramics prepared by solid-state reaction. $NB_{0.50}T$ prepared by anatase TiO_2 is insulating, whereas that prepared by rutile TiO_2 is ionically conductive. Possible reasons for the dramatic impact of TiO_2 polymorph on the electrical properties of $NB_{0.50}T$ are discussed below.

"Accidental" doping from impurities in the raw materials

Previous studies[9, 14, 15, 26, 27] show low levels of acceptor-doping, such as Na^+, Li^+, K^+, Ca^{2+}, Sr^{2+}, Ba^{2+} to replace Bi^{3+} on A-site, and Mg^{2+}, Zn^{2+}, Sc^{3+}, Al^{3+}, Fe^{3+}, and Ga^{3+} to replace Ti^{4+} on B-site, can create oxygen vacancies in NBT by an ionic compensation mechanism, and consequently introduce high-levels of oxide-ion conductivity into NBT. On the contrary, low levels of donor-type dopants such as Nb^{5+}, Ta^{5+} can fill oxygen vacancies to suppress oxide-ion conduction. For example, 0.5%Nb-doping on the Ti-site can change the electrical conduction mechanism of NBT from high oxide-ion to low electronic conduction[28]. In this work, two groups of NBT samples, i.e., NBT_111 and NBT_112, NBT_333 and NBT_334, were prepared using the same Na_2CO_3 and Bi_2O_3 but different TiO_2 reagents. They present dramatically different electrical properties: NBT ceramics prepared using the rutile phase TiO_2-1 (99.9%) and TiO_2-3 (99.9%) are conductive; those prepared using the anatase phase TiO_2-2 (99.6%) and TiO_2-4 (99.99%) are insulating. Although Fig.4 shows σ_b is independent of the grade purity, it is still necessary to clarify the impurity elements in the TiO_2 reagents, in particular, whether donor-type elements are presented in anatase TiO_2-2 and TiO_2-4.

The dominant impurity elements of these four types of TiO_2 from their Certificate of Analysis (CoA) provided by the suppliers are listed in Table 3. Many impurities in TiO_2-1, TiO_2-2, and TiO_2-3 are acceptor-type elements. Donor-type impurities such as Nb, Ta, and V are absent or below 10 ppm. Compared to TiO_2-1, TiO_2-2 has a significantly higher level of K impurity. The effect of K on σ_b of NBT has been previously investigated by intentional doping of K to replace either Bi^{3+} or Na^+ on the A-site of NBT[15,16]. Acceptor-doping of K^+ to replace Bi^{3+} creates oxygen vacancies to enhance oxide-ion conductivity. In contrast, partial replacement of Na^+ by K^+ decreases σ_b, which is attributed to the more significant K-loss than Bi-loss during sintering, and therefore makes K-doped NBT Bi-rich on the A-site. For NBT_112, if all the K impurities in TiO_2-2 replace Na, the nominal composition of NBT can be written as $Na_{0.498844}K_{0.001156}Bi_{0.5}Ti_{0.998844}O_{3-\delta}$. Under our processing route, the Bi-loss was previously estimated to be in the range of 0.0017-0.0033, corresponding to a formula of $Na_{0.5}Bi_{04967-0.4983}TiO_{2.995-2.9975}$[29]. Assuming a complete loss of K during sample preparation, the nominal composition of the prepared NBT is $Na_{0.498844}Bi_{04967-0.4983}Ti_{0.998844}O_{3-\delta}$, which can be considered as Bi-deficient NBT and should present oxide-ion conduction behaviour. Consequently, the relatively high level of K impurities in TiO_2-2 is not sufficient to explain the insulating behavior of NBT_112.

The COA of the high-purity TiO_2-4 (99.99%) suggests a total metallic impurity level of 97 ppm without specifying the impurity elements. If we assume all the impurities in TiO_2-4 are donor-type dopants (i.e., Nb^{5+}), the prepared ceramics corresponds to 0.01% Nb-doped NBT. Our previous study[27] showed 0.2% Nb-doping can only partially fill the oxygen vacancies in NBT ceramics prepared by our "standard" route. 0.2% Nb-doped NBT presents mixed ionic-electronic conduction behavior with E_a ~ 0.9 eV and t_{ion} ~ 0.5. Therefore, 0.01% Nb-doping is insufficient to fully eliminate oxygen vacancies to result in predominant electronic conduction behavior of NBT_334.

To conclude the above, "accidental" donor-doping from anatase TiO_2 (TiO_2-2 and TiO_2-4) is not the dominant reason for the electrically insulating behavior of NBT_112 and NBT_334. Alternative reason(s) need to be considered.

Table 3 Major metallic impurities (>10 ppm) in TiO_2 reagents.

TiO_2	Na	K	Ca	Mg	Zn	Al	Cr	Pb	Pd	Pt
TiO_2-1		45.5					23.9	13.4	25.8	18.5
TiO_2-2	36	1156	< 20			50				
TiO_2-3	<100	<100	<100	<100	<100	<100				
TiO_2-4	Unspecified, total metallic impurities 97 ppm									

Formation process of NBT

Our previous studies[4, 5] show the oxide-ion conductivity of undoped $NB_{0.50}T$ originates from the oxygen vacancies generated by Bi-loss during ceramic processing. The insulating $NB_{0.50}T$ prepared using anatase TiO_2 suggests a lower amount of Bi-loss than the conductive $NB_{0.50}T$ prepared using rutile TiO_2. During solid state processing, there are several possible sources for Bi-loss, including the following. (1) Bi_2O_3 loss caused by materials transfer from the milling bottle to beaker. Although carefully rinsed using isopropanol several times after the first round of ball milling, small amounts of Bi_2O_3 powder may still stick on the inner side of the milling bottle or on the surfaces of the milling balls. (2) Volatility of Bi_2O_3 during calcination. To form NBT, the ball-milled and sieved Na_2CO_3, Bi_2O_3, and TiO_2 mixture is heated from room temperature to 800 °C, where solid-state reaction of the reagents takes place to form NBT perovskite. The polymorphism of TiO_2 (rutile or anatase) may influence the reaction pathway or reaction rate for NBT formation and consequently may result in different levels of Bi_2O_3 loss. (3) Volatility of Bi_2O_3 during sintering. After calcination, single-phase NBT with a perovskite structure has formed. To prepare dense ceramics, green bodies of pressed NBT pellets are subjected to sintering at 1150 °C. Although fully embedded in sacrificial powder, exposure to such high temperature may induce Bi-loss of NBT considering its volatility.

In the three above-mentioned possible sources, if there is any Bi-loss in (1) and (3), it should be similar for both rutile and anatase TiO_2 as we have followed a strict processing route for the NBT preparation. It is, therefore, necessary to investigate the NBT formation process during heating to identify the possible impact of rutile and anatase TiO_2 on the reaction pathway or reaction rate. For this purpose, the ball-milled and sieved mixtures of pre-dried Na_2CO_3, Bi_2O_3, and TiO_2 (TiO_2-3 and TiO_2-4) were calcined between 400-800 °C (at 50 °C increments) for 2 h and the reaction products identified by both laboratory and synchrotron XRD. The formation process of NBT during solid-state reaction was previously investigated by Aksel and Jones using *in situ* high-temperature diffraction[30]. In their study, anatase TiO_2 powder (without pre-drying) was mixed with Na_2CO_3 and Bi_2O_3 and heated continuously from room temperature to 700 °C with a ramp rate of 4 °C min^{-1}. Two transient phases ($Bi_{12}TiO_{20}$ and $Bi_4Ti_3O_{12}$) were observed at 500-650 °C. In our work, the mixed powder was held at each temperature for 2 h to allow a longer reaction time than *in situ* heating for easier identification of the reaction products.

Full synchrotron XRD patterns of the calcined powder in the 2θ range of 15-80° are shown in Fig.S3 and the patterns in a narrower 2θ range between 20-50° displayed in Figure 5. Evolution of the XRD pattern with increasing calcination temperature in the case of rutile TiO_2 is presented in Fig.5a. At 500 °C, the XRD pattern is dominated by peaks corresponding to α-Bi_2O_3. Peaks for rutile TiO_2 at 2θ~27.5 (partially overlapping with one from Bi_2O_3), 36, 39.2, 41.2, and 44° can also be identified. A weak peak at 2θ~30.1° corresponds to the (002) reflections of the monoclinic phase of Na_2CO_3. At 550 °C, apart from the reagent peaks, a weak peak at 2θ~32.8° from the (321) reflections of Sillenite $Bi_{12}TiO_{20}$ can be detected. At 600 °C, the (310) peak for $Bi_{12}TiO_{20}$ at 2θ~27.7°appears and NBT perovskite peaks (2θ~23, 32.5, 40 and 47°) start to appear. At 650 °C, the XRD pattern is dominated by peaks from NBT perovskite with two weak peaks from $Bi_{12}TiO_{20}$. At 700 and 800 °C, only NBT peaks can be detected, suggesting the reaction is complete. In the case of anatase TiO_2, as shown in Fig.5b, the reaction starts at 550 °C, as indicated by the peak at 2θ~27.7°, corresponding to diffraction from the (310) planes of $Bi_{12}TiO_{20}$. At 600 °C, the NBT perovskite starts to form with the presence of a significant amount of sillenite $Bi_{12}TiO_{20}$. At 650 °C, the diffraction pattern is dominated by $Bi_{12}TiO_{20}$ and NBT, with one small peak from unreacted TiO_2 at 2θ~25.4°. The sillenite phase is still present at 700 °C. Single phase NBT is obtained after calcination at 800 °C.

As summarized in Table 4, the most significant difference in the formation process of NBT prepared by rutile and anatase TiO_2 is the $Bi_{12}TiO_{20}$ phase formed at intermediate temperatures. When using rutile TiO_2, only a small amount of $Bi_{12}TiO_{20}$ is detected at 550-650 °C. In contrast, when using anatase TiO_2, a large amount of $Bi_{12}TiO_{20}$ is formed during heating and is present over a wider temperature range up to 700 °C.

Recent studies by Thong *et al.*[31, 32] have suggested the chemical reaction among Na_2CO_3, K_2CO_3, and Nb_2O_5 during formation of $(K,Na)NbO_3$ perovskite is strongly dependent on the size of Nb_2O_5 precursor. To elucidate the impact of rutile and anatase TiO_2 on NBT formation, particle size analysis was conducted on TiO_2 reagents and the ball-milled mixture prior to calcination. As shown in Fig.S4a and 4b, the particle size of raw TiO_2, both rutile and anatase, shows a wide distribution between 0.1 to 1000 μm due to different levels of particle agglomeration. After ball milling (Fig.S4c and 4d), mixtures with rutile TiO_2 and anatase TiO_2 both show a single, normal distribution of particle size with an average value of 4.51 and 4.61 μm, respectively. The different formation process of NBT using rutile and anatase TiO_2 is, therefore, a polymorphic effect and not a particle size effect.

The reason(s) why anatase TiO_2 is more beneficial to the formation of the $Bi_{12}TiO_{20}$ phase during solid-state reaction is beyond the scope of this paper but is worthy of further in-depth investigation based on variations in crystal structure, thermodynamics, and reaction kinetics. The key information extracted from Fig.5 is formation of NBT by solid-state reaction among Na_2CO_3, Bi_2O_3, and TiO_2 is a competition between the following two reactions:

$$6Bi_2O_3 + TiO_2 \rightarrow Bi_{12}TiO_{20} \quad (1)$$

$$0.25Na_2CO_3 + 0.25Bi_2O_3 + TiO_2 \rightarrow Na_{0.5}Bi_{0.5}TiO_3 + 0.25CO_2(g) \quad (2)$$

In Equation (1), 1 mole of TiO_2 reacts with 6 moles of Bi_2O_3 to form $Bi_{12}TiO_{20}$; in Equation (2), 1 mole of TiO_2 reacts with 0.25 moles of Bi_2O_3 to form NBT. Here we calculated a parameter (*f*) from the intensity of the strongest peak from the XRD patterns of Bi_2O_3, $Bi_{12}TiO_{20}$, and NBT according to

$$f_{Bi_2O_3} = \frac{I_{Bi_2O_3,2\theta\sim27.5^\circ}}{I_{Bi_2O_3,2\theta\sim27.5^\circ}+I_{Bi_{12}TiO_{20},2\theta\sim27.7^\circ}+I_{NBT,2\theta\sim32.6^\circ}} \times 100\% \quad (3a)$$

$$f_{Bi_{12}TiO_{20}} = \frac{I_{Bi_2O_3,2\theta\sim27.5^\circ}}{I_{Bi_2O_3,2\theta\sim27.5^\circ}+I_{Bi_{12}TiO_{20},2\theta\sim27.7^\circ}+I_{NBT,2\theta\sim32.6^\circ}} \times 100\% \quad (3b)$$

$$f_{NBT} = \frac{I_{Bi_2O_3,2\theta\sim27.5^\circ}}{I_{Bi_2O_3,2\theta\sim27.5^\circ}+I_{Bi_{12}TiO_{20},2\theta\sim27.7^\circ}+I_{NBT,2\theta\sim32.6^\circ}} \times 100\% \quad (3c)$$

as an indicator of relative change of Bi_2O_3 content in these three Bi-containing phases. (Please note, for accurate calculation of the mass fraction, a mass absorption coefficient for each phase should be considered. Here a simplified fraction is used to show the trends). Variation of f_{Bi2O3} with temperature is presented in Fig.S5a, where a faster drop of f_{Bi2O3} can be observed when anatase TiO_2 is used. At 600 °C, f_{Bi2O3} values are ~35% in the mixture with anatase TiO_2 and this is significantly lower than ~65% in the mixture with rutile TiO_2. Sublimation of Bi_2O_3 below its melting temperature has been previously investigated by Cheng *et al.*[33]. They tested the mass loss of Bi_2O_3 at 650 °C in an air box furnace for different holding times up to 100 h, and reported ~ a 0.125% mass loss of Bi_2O_3 after 5 h. The mass loss of Bi_2O_3 was effectively reduced by SnO_2-doping. 1% and 10% Sn-doping reduced the mass loss to 0.05 and < 0.01%, respectively. Therefore, when NBT is prepared using anatase TiO_2, formation of a large amount of $Bi_{12}TiO_{20}$ phase can effectively immobilise Bi_2O_3 to reduce its sublimation and consequently prohibits creation of oxygen vacancies to result in insulating behavior of NBT.

The atomic fractions of Na, Bi, and Ti of NBT prepared from rutile and anatase TiO_2, in the form of calcined powder and dense ceramics, were determined by ICP-AES analysis and are listed in Table 5. Calcined powder and sintered pellets of NBT prepared by rutile TiO_2 show a Na/Bi ratio > 1, and those prepared by anatase TiO_2 show a Na/Bi ratio < 1. This gives evidence for the reduced Bi-loss during calcination of NBT when anatase TiO_2 is used.

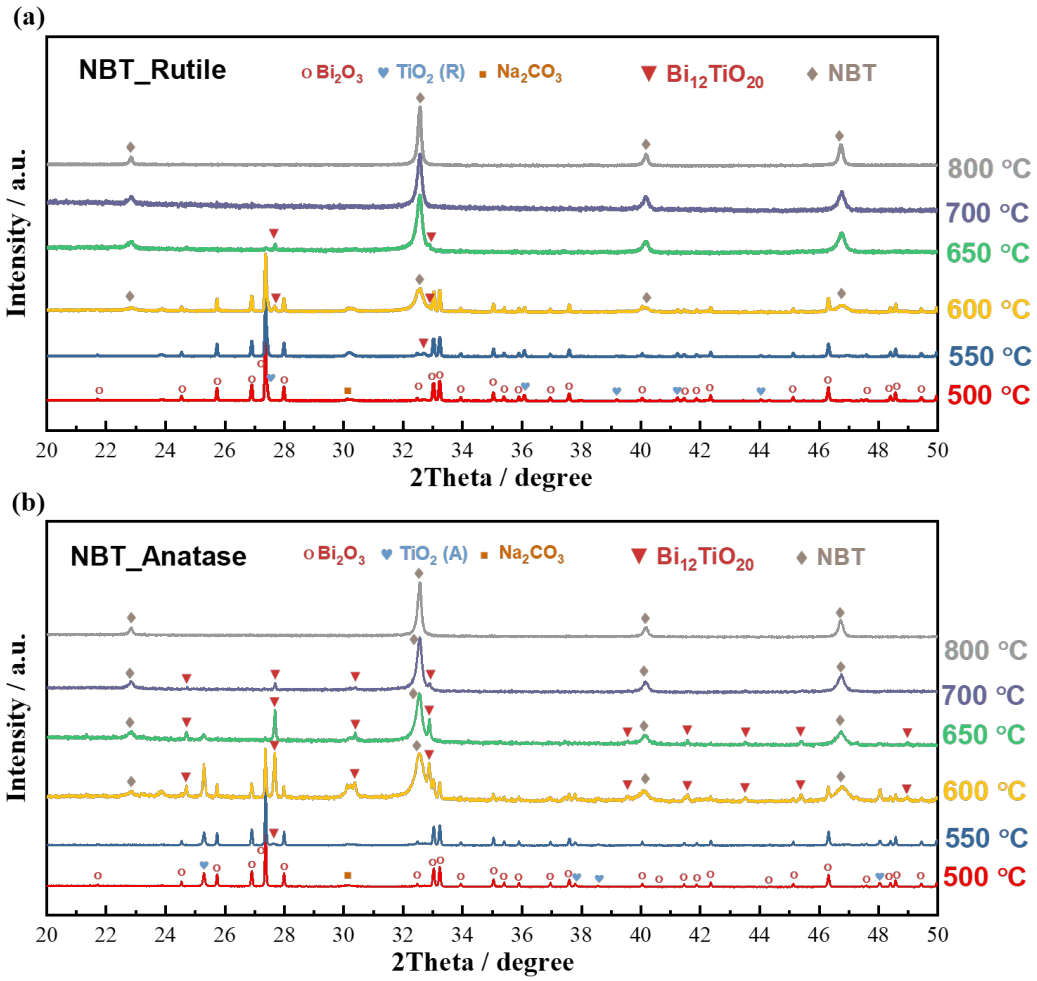

Fig.5 Synchrotron XRD patterns of the Na_2CO_3, Bi_2O_3 and TiO_2 mixtures after heat treatment at 500-800 °C (at increments of 50 °C) for 2 h: (a) Rutile TiO_2 and (b) anatase TiO_2.

Table 4 Reaction products at each temperature identified by synchrotron XRD. "weak" and "strong" are defined according to the peak intensity relative to the strongest peak on each pattern. Very weak: < 5%; weak: 10-20%; strong: 50-90%; very strong: > 90%.

TiO_2 polymorph	Product	Temperature / °C					
		500	550	600	650	700	800
Rutile	Na_2CO_3	√	√	√			
	Bi_2O_3	√	√	√	√		
	TiO_2	√	√	√			
	$Bi_{12}TiO_{20}$		√, very weak	√, weak	√, weak		
	NBT			√	√	√	√
Anatase	Na_2CO_3	√	√	√			
	Bi_2O_3	√	√	√			
	TiO_2	√	√	√	√		
	$Bi_{12}TiO_{20}$		√, very weak	√, very strong	√, strong	√, weak	
	NBT			√	√	√	√

Table 5 Atomic fractions of Na, Bi, and Ti in the calcined powder and sintered ceramics of NBT prepared by rutile and anatase TiO_2. The numbers are the average value from 3 ICP-AES tests.

	TiO_2 Polymorph	Na / %	Bi / %	Ti /%	Na/Bi
Calcined powder	Rutile	25.75	25.28	48.97	> 1
	Anatase	24.23	25.82	49.95	< 1
Sintered ceramics	Rutile	25.43	24.76	49.80	> 1
	Anatase	24.47	25.08	50.46	< 1

The above analysis suggests rutile and anatase TiO_2 have different abilities to pre-react and "trap" Bi_2O_3 in the solid-state reaction with Na_2CO_3 and TiO_2. To further support the above statement, an additional NBT ceramic sample was prepared using a mixture of rutile and anatase TiO_2 with a weight ratio of 1:1 following the same processing route (denoted as NBT_$R_{0.5}A_{0.5}$). Fig. 6 compares the microstructure of NBT_R, NBT_A, and NBT_ $R_{0.5}A_{0.5}$. The ionic conductive NBT_R has large grains (~ 15-20 μm, Fig.6a), the insulating NBT_A shows small grains (~ 1-2 μm, Fig.6b). This is consistent with the empirical conductivity-grain size relationship summarized in Ref.13. NBT_ $R_{0.5}A_{0.5}$, as shown in Fig.6c, displays a random mixture of large (~ 5 μm) and small (~ 1 μm) grains. Although the large grains in NBT_ $R_{0.5}A_{0.5}$ are much smaller than those in NBT_R possibly because the grain growth is inhibited by the neighbouring small grains, the distinguishable presence of two types of grains gives additional evidence that rutile and anatase TiO_2 react independently with Bi_2O_3 and Na_2CO_3 during NBT formation.

σ_b of NBT_ $R_{0.5}A_{0.5}$ was estimated from Z^* and M''-log$f$ plots (Fig.S5) and plotted as a function of 1000/T, as shown in Fig.6d. σ_b of NBT_ $R_{0.5}A_{0.5}$ is intermediate to that of NBT_R and NBT_A, with a change of E_a from 0.51 eV (300-550 °C) to 0.76 eV (550-750 °C). In the lower temperature range, the small grains are too insulative to contribute to electrical conduction. Therefore, σ_b is dominated by the large, conductive grains and thus presents an E_a similar to that of NBT_R. With increasing temperature, the small grains also contribute to electrical conduction to result in an increase in E_a. The ceramic microstructure and electrical conductivity of NBT_$R_{0.5}A_{0.5}$ further support our conclusion that the dramatically different electrical behavior of NBT_R and NBT_A originate from the use of different TiO_2 polymorphs in the solid-state preparation of NBT.

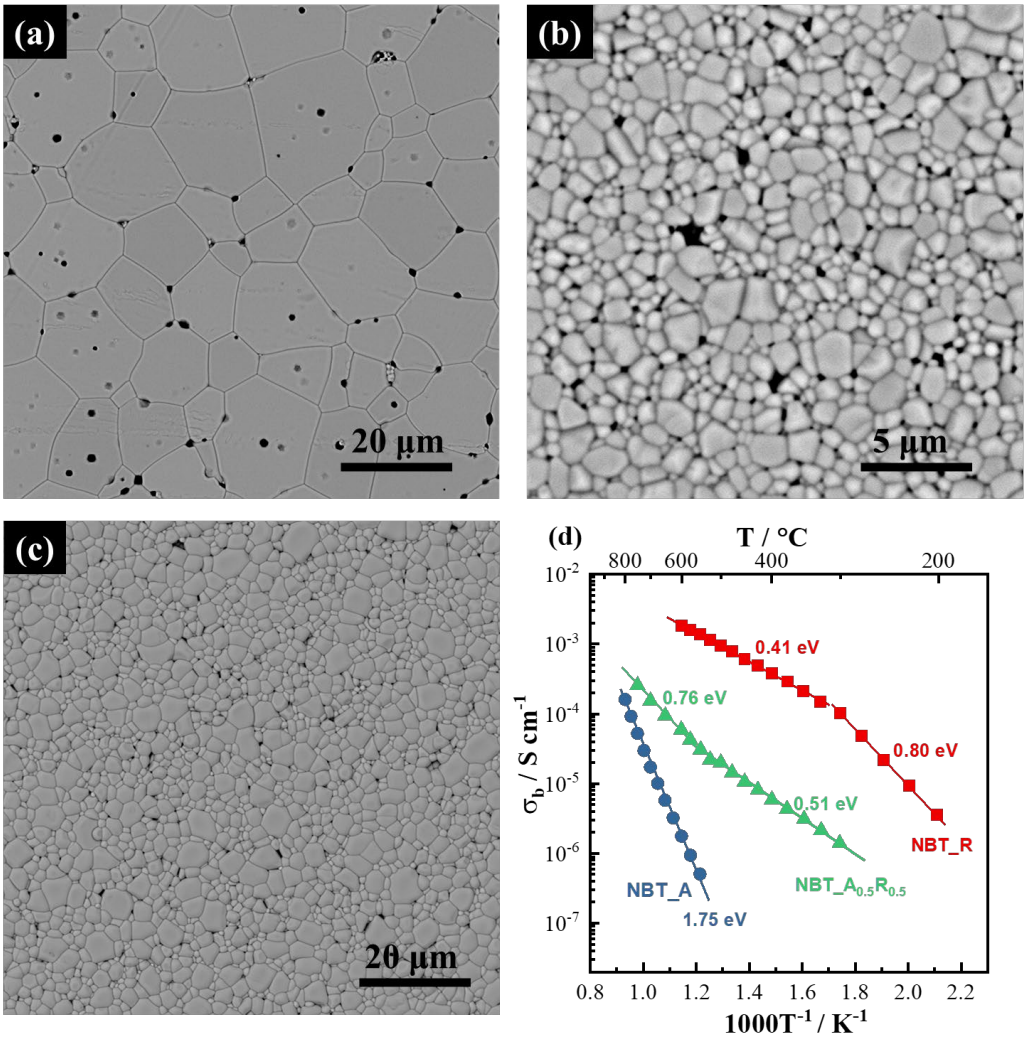

Figure 6. (a)-(c) SEM micrographs of thermally etched surfaces of NBT_R, NBT_A and NBT_$R_{0.5}A_{0.5}$, respectively. (d) Arrhenius plots for σ_b of NBT_R, NBT_A and NBT_$R_{0.5}A_{0.5}$. The numbers in eV are the E_a values.

Perspectives on the reproducible synthesis of NBT by solid-state processing

Solid-state reaction is the most readily available and economical method for large-scale production of NBT-based materials. As σ_b of NBT is highly sensitive to small compositional variations, it is essential to follow a strict processing procedure and to be aware of the influence of reagent grade purity and polymorphism on the reaction mechanism and final electrical properties. Particular attention should be given to the following: 1) pre-drying of the raw reagents. This is not only important to guarantee precise weighing of the reagents to control the starting NBT stoichiometry but also to know the polymorphism of the dried TiO_2 reagent. 2) The grade purity of the raw reagents. The reagents used in this work all have reasonably high purity (>99.5%). If low purity reagents are used to prepare NBT, it is necessary to consider the possible impact from "accidental" doping from any high-level impurity elements. 3) The polymorphism of any dried TiO_2 reagents used prior to milling and mixing. Given the sensitivity of the anatase to rutile polymorphic transition on low levels of impurities, it is conceivable that batches of TiO_2 from the same supplier may show variations in their anatase to rutile content after drying at 900 °C.

Finally, it is worth mentioning that although σ_b of NBT can be tuned by manipulating the Na/Bi ratio or by chemical doping, the ability of accommodating A-site Na (or Bi) nonstoichiometry or dopants can be very low in NBT. Our previous studies[4, 24, 27] have shown the presence of Na,Ti-rich secondary phase(s) in Bi-deficient NBT ($NB_{0.49}T$) or acceptor-doped NBT (Mg-doped NBT) and Bi-rich secondary phase(s) in Bi-excess NBT ($NB_{0.51}T$) and Nb-doped NBT. Nominally stoichiometric NBT is usually cleaner than the above mentioned non-stoichiometric or doped NBTs[4]. To avoid possible impact from secondary phases on the materials properties, in many circumstances a nominally stoichiometric NBT is preferred. Therefore, to make sure the conductivity meets the requirement for different applications, it is suggested rutile TiO_2 should be used to prepare ionically conducting NBT, and anatase TiO_2 for preparing insulating NBT.

Conclusion

The dramatic impact of the TiO_2 polymorph on the electrical conductivity and conduction mechanisms of nominally stoichiometric NBT ceramics ($NB_{0.50}T$) prepared by solid-state

reaction method is reported. Based on our processing route, NBT ceramics prepared using rutile TiO_2 are ionically conductive, and those prepared using anatase TiO_2 are electrically insulating. The dramatic difference in electrical properties of NBT prepared using rutile and anatase TiO_2 is strongly linked to the NBT formation process: the intermediate, Bi-rich Sillenite phase $Bi_{12}TiO_{20}$ is more stable and forms in larger amounts during formation of NBT when anatase TiO_2 is used. The intermediate $Bi_{12}TiO_{20}$ immobilises significant amounts of Bi_2O_3 and therefore reduces Bi_2O_3-loss during heating, and consequently lowers the oxygen vacancy concentration to suppress oxide-ion conduction in NBT prepared by anatase TiO_2. This work provides a plausible explanation for the large variation of σ_b for NBT reported in the literature and highlights the importance of selecting appropriate TiO_2 reagents to obtain controllable σ_b in NBT-based ceramics. For ion-conducting applications, rutile TiO_2 should be used, and for dielectric applications anatase TiO_2 should be used. Furthermore, any study of the effect of additional doping with foreign elements on NBT or solid solutions with NBT should start with anatase TiO_2. This work also demonstrates the importance of understanding the solid-state reaction mechanisms in the formation and compositional control of NBT.

Conflicts of interest

There are no conflicts to declare.

Acknowledgements

The authors thank National Natural Science Foundation of China (52072239, 22002089, 51971138), EPSRC (EP/L027348/1), Foundation of China-Excellent Young Scholars (51922068), Shanghai Pujiang Program No. 19PJ1404400 for funding.

References

1 E. Aksel, J. L. Jones, Sensors 2010, **10,** 1935.
2 D. Damjanovic, N. Klein, J. Lin, V. Porokhonskky, Funct. Mater. Lett. 2010, **3**, 5.
3 X. Zhou, G. Xue, H. Luo, C. R. Bowen, D. Zhang, Prog. Mater. Sci. https://doi.org/10.1016/j.pmatsci.2021.100836.
4 M. Li, M. J. Pietrowski, R. A. De Souza, H. Zhang, I. M. Reaney, S. N. Cook, J. A. Kilner, D. C. Sinclair, Nat. Mater. 2004, **13**, 31.
5 M. Li, H. Zhang, S. N. Cook, L. Li, J. A. Kilner, I. M. Reaney, D. C. Sinclair, Chem. Mater. 2015, **27**, 629.
6 D. K. Khatua, T. Mehrotra, A. Mishra, B. Majumdar, A. Senyshyn, R. Ranjan, Acta Mater. 2017, **134**, 177.
7 L. Li, PhD Thesis, The University of Sheffield, 2017.
8 X. Chen, J. Zeng, X. Yan, M. Zhou, P. Tang, T. Liang, W. Li, Solid State Ionics 2017, **309**, 152.
9 L. Koch, S. Steiner, K. C. Meyer, I. T. Seo, K. Albe, T. Frömling, J. Mater. Chem. C 2017, **5**, 8958.
10 F. Yang, P. Wu, D. C. Sinclair, J Mater. Chem. C 2017, **5**, 7243.
11 Y. Lu, C. A. López, J. Wang, J. A. Alonso, C. Sun, J. Alloys Compd. 2018, **752**, 213.
12 R. Bhattacharyya, S. Omar, Solid State Ionics 2018, **317**, 115.
13 F. Yang, J. S. Dean, Q. Hu, P. Wu, E. Pradal-Velázquez, L. Li, D. C. Sinclair, J. Mater. Chem. A 2020, **8** ,25120.
14 S. Steiner, I. T. Seo, P. Ren, M. Li, D. J. Keeble, T. Frömling, J. Am. Ceram. Soc. 2019, **102**, 5295.
15 F. Yang, M. Li, L. Li, P. Wu, E. Pradal-Velázquez, D. C. Sinclair, J. Mater. Chem. A 2017, 5, 21658.
16 F. Yang, M. Li, L. Li, P. Wu, E. Pradal-Velázquez, D. C. Sinclair, J Mater. Chem. A 2018, **6**, 5243.
17 N. H. Chan, R. K. Sharma, D. M. Smyth, J. Am. Ceram. Soc. 1981, 64, 556.
18 L. Li, B. Walkley, I. M. Reaney, D. C. Sinclair, J. Euro. Ceram. Soc. 2021, **41**, 4189.
19 N. T. Nolan, M. K. Seery, S. C. Pillai, J. Phys. Chem. C 2009, **113**, 16151.
20 D. A. H. Hanaor, C. C. Sorrell, J. Mater. Sci. 2011, **46**, 855.
21 C. Goutham, K. V. A. Kumar, S. S. K. Raavi, C. Subrahmanyam, S. Asthana, J. Materiomics https://doi.org/10.1016/j.jmat.2021.06.003.
22 K. Reichmann, A. Feteira, M. Li, Materials 2015, **8**, 8467.
23 F. Yang, H. Zhang, L. Li, I. M. Reaney, D. C. Sinclair, Chem. Mater. 2016, **28**, 5269.
24 F. Yang, P. Wu, D. C. Sinclair, Solid State Ionics 2017, **299**, 38.
25 M. Bousquet, J.-R. Duclère, E. Orhan, A. Boulle, C. Bachelet, C. Champeaux, J. Appl. Phys. 2010, **107**, 104107.
26 D. P. C. Shih, A. Aguadero, S. J. Skinner, Solid State Ionics 2018, **317**, 32.
27 R. Bhattacharyya, S. Omar, J. Alloys Compd. 2018, 746, 54.
28 L. Li, M. Li, H. Zhang, I. M. Reaney, D. C. Sinclair, J. Mater. Chem. C 2016, **4**, 5779.
29 M. Li, L. Li, J. Zang, D. C. Sinclair, Appl. Phys. Lett. 2015, **106**, 102904.
30 E. Aksel, J. L. Jones, J. Am. Ceram. Soc. 2010, **93**, 3012.
31 H. Thong, C. Zhao, Z. Zhu, X. Chen, J. Li, K. Wang, Acta Mater. 2019, **166**, 551.
32 H. Thong, A. Payne, J. Li, Y. Cheng, J. L. Jones, K. Wang, Acta Mater. 2021, **211**, 116833.
33 Y. Cheng, Y. Chen, W. J. Wei, J. Ceram. Process. Res. 2018, **19**, 388.